Differential reflectivity spectroscopy on single patch nanoantennas

Juan Uriel Esparza Villa, Amit Raj Dhawan, Rafael Salas-Montiel, Willy Daney de Marcillac, Bruno Gallas, Agnès Maitre, Jean-Marc Frigerio

▶ **To cite this version:**

Juan Uriel Esparza Villa, Amit Raj Dhawan, Rafael Salas-Montiel, Willy Daney de Marcillac, Bruno Gallas, et al.. Differential reflectivity spectroscopy on single patch nanoantennas. Applied Physics Letters, 2020, 117 (23), pp.231102. 10.1063/5.0029596 . hal-03095850

HAL Id: hal-03095850

https://hal.sorbonne-universite.fr/hal-03095850

Submitted on 4 Jan 2021

HAL is a multi-disciplinary open access archive for the deposit and dissemination of scientific research documents, whether they are published or not. The documents may come from teaching and research institutions in France or abroad, or from public or private research centers.

L'archive ouverte pluridisciplinaire **HAL**, est destinée au dépôt et à la diffusion de documents scientifiques de niveau recherche, publiés ou non, émanant des établissements d'enseignement et de recherche français ou étrangers, des laboratoires publics ou privés.

Differential reflectivity spectroscopy on single patch nanoantennas

Juan Uriel Esparza,[1] Amit Raj Dhawan,[1] Rafael Salas-Montiel,[2] Willy Daney de Marcillac,[1] Jean-Marc Frigerio,[1] Bruno Gallas,[1] and Agnès Maître[1, a)]

[1)] *Sorbonne Université, CNRS, Institut des Nanosciences de Paris, UMR 7588, 75005 Paris, France*

[2)] *Department of Physics, Mechanics, Materials and Nanotechnology, L2n CNRS ERL 7004, Université de Technologie de Troyes, 12 rue Marie Curie, 10004, Troyes, France*

(Dated: 11 November 2020)

We present an experimental technique adapted to characterize individual metallic nanostructure in terms of differential reflectivity spectroscopy. We analyze gold patch nanoantennas holding different morphological properties. Our experimental methodology shows steady and reliable results consistent with classical analytical approximations and simulation methods. This technique allows to identify absorption properties of metallic nanostructures commonly associated to surface plasmon resonances. By contrasting the light absorbed solely by the metallic antenna with respect to a surrounding reference medium, we found that some antennas show absorption of almost 50% of the incident light across the range of the visible spectrum. Plasmonic patch nanoantennas are promising systems in which the confinement of the electromagnetic field inside the dielectric gap strongly modify the local density of states.

Differential reflectivity spectroscopy (DRS) is a non-destructive, surface analytical technique used to identify the optical absorption signature of samples with a reflecting substrate, within a given spectral range from the near-UV to the IR region. The comparison of the sample under investigation with a reference, under same conditions of illumination, provides sensitive spectral information, so that, even the smallest inhomogeneity change between samples may lead to a different reflectogram signature. As a consequence, DRS has been used for several purposes such as the study of intrinsic and doping materials (n- or p-type)[1], the formation of metallic clusters during thin vapor deposition[2–4], the anisotropy in metallic surface structure[5,6] and analysis of multi-polar effects in alkali metals such as potassium nanoparticles[7,8]. In addition, DRS technique can also probe the optical properties of individual plasmonic nanostructures[9]. DRS technique offers an straightforward implementation and an alternative with respect to others optical surface techniques[10] such as transmission spectroscopy[11], dark-field microscopies[12], spatial modulation spectroscopy[13,14].

In the present work, we propose a DRS technique for the analysis of differential reflectivity on single metallic nanoantennas exhibiting plasmonic resonances which are highly dependent on the morphological properties of the particle and the surrounding medium[15–17]. Thanks to this spectroscopic technique, we measure the plasmonic signature of individual patch nanoantennas with different morphological features across the visible spectral range.

We fabricated 4x4 matrix of gold (Au) nanopatch supported by a 40 nm poly(methyl methacrylate) (PMMA), with index of refraction n = 1.45, deposited on a Au substrate using an in-situ laser etching lithography technique inspired by[18] and described in reference[19]. The spectroscopic ellipsometry data for the gold permittivity are plotted in supporting information (Fig. **??**). The Au patches are disks with a 20 nm thickness and a typical diameter of 1 μm. Fig. 1a shows a scanning electron microscope (SEM) image of 16 patch antennas. Although they were fabricated with the same lithographic parameters, they exhibit slightly different morphological properties (diameter, defects, etc.), probably due to inhomogeneities in the resist layers used for the photolithography and to lift-off processes. In Fig. 1b, we show a scanning electron microscope image corresponding to antenna 9. We note that the nanodisk is not perfectly circular. Indeed, the patch has a slight asymmetry and the border edge is discontinuous. Therefore, we define an effective diameter d_{eff} as the diameter of the patch disk not taking into account asymmetries and defects of the nanostructures (yellow circumference on Fig. 1b). We found that the effective diameter of antenna 9 corresponds to a diameter $d_{\text{eff}} = 830$ nm.

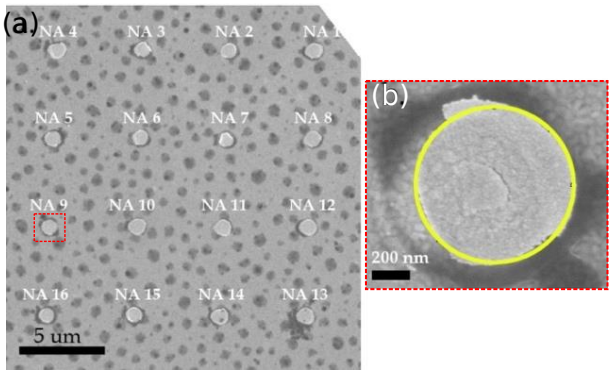

FIG. 1. Gold patch antennas. Scanning electron microscope image of (a) an array of 4x4 gold patch antennas laying on gold substrate and (b) zoom around nanoantenna 9. The effective diameter is $d_{\text{eff}} = 830$ nm (limited by a yellow circle). Scale bar is 5 μm and 200 nm in (a) and (b), respectively.

[a)] Electronic mail: agnes.maitre@insp.upmc.fr

The experimental setup consists of a confocal reflection microscope with a halogen lamp as a source of light (Fig. 2). The wide-spectrum lamp (ranging from 350 to 800 nm) is partially reflected by a 50:50 beam splitter inside the microscope. The reflected light is then focused by an objective (0.80 NA and 100x), which illuminates the sample. The field of view of the optical system has a diameter of 0.265 mm. The light reflected by the sample is then collected by the same objective and focalized in the aperture of a circular pinhole of 100 μm diameter. The pinhole, placed at the conjugated image plane of the sample, is employed as a spatial filter to reject most of the light reflected by the sample and to collect exclusively the light reflected by a 1 μm disk centered on the nanodisk. The lateral precision for positioning the pinhole is estimated to be 5 μm that corresponds in the conjugated plane, where the sample lies, to 50 nm. The reflected light is then collimated and coupled to an optical fiber connected to a Jobin Yvon HR 460 spectrometer equipped with a 150 g/mm grating. The linear dispersion of our instrument is 14.1 [nm/mm], corresponding to 0.36 [nm/px] taking into account the physical size of the spectrometer CCD.

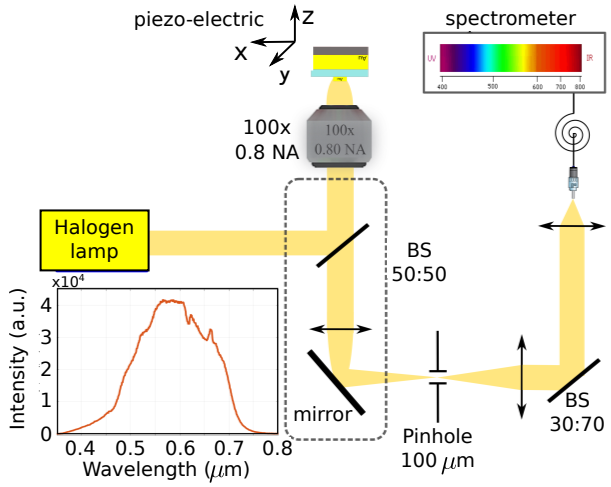

FIG. 2. Experimental setup used to perform specular reflectivity measurements. The confocal reflection microscope collects the light reflected from the individual antennas. Inset: spectrum of the halogen source.

For differential reflectivity spectroscopy technique, the lamp is first switched off and replaced by a 405 nm laser diode that illuminates the sample on a 500 nm radius spot size. The sample is raster scanned across the xy-plane and the fluorescence is collected within the spectral range ranging from 584 nm to 676 nm in order to obtain a spectroscopic cartography of the fluorescence.

Fluorescence imaging helps to distinguish the Au nanodisk from another materials surrounding the antenna. Figure 3a shows a fluorescence scanning image of a single Au patch antenna of 945 nm effective diameter. In the image we traced a circle of 1 μm diameter indicating the area collected by the spatial filter. From the image,

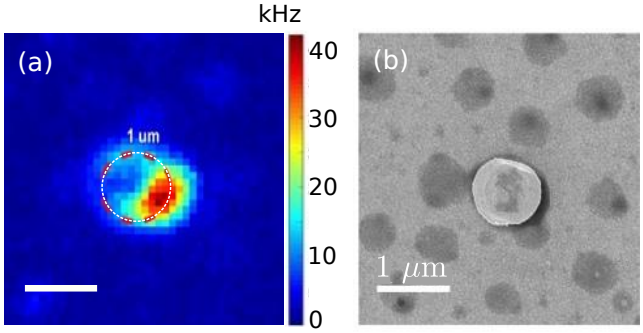

FIG. 3. Identification of the patch antenna with scanning fluorescence imaging. (a) Scanning laser fluorescence image of a patch nanoantenna. The bright spot is generated at an edge defect that efficiently scattered light. (b) Corresponding scanning electron microscope image of the single patch nanoantenna in (a). The opaque dots around the patch antenna are lift-off resist residuals from the fabrication process.

we observe a bright spot generated at the bottom right edge defect of the patch antenna that efficiently scatters light. Furthermore, we note low-level fluorescence dots around the patch antenna from lift-off resist that remains from the fabrication process[20]. Figure 3b shows the corresponding SEM image of the same nanoantenna. From both images we can correlate the bright fluorescence spot of Fig. 3a with the edge defect observed in Fig. 3b. Finally, we can identify in both the fluorescence and SEM images the position of the patch antenna.

Once the antenna is identified by fluorescence imaging, we switch the illumination source and replace the laser by the white lamp. We register the reflected spectra at two positions on the sample. In the first one, the microscope pinhole is optically conjugated to the patch antenna. In the second one, pinhole is conjugated with a zone some micrometers far away from the antenna, acting as reference. We define the differential reflectivity spectroscopy (DRS) as the relative light reflected by antenna with respect to the reference:

$$DRS = \frac{\Delta R_{\text{ant}}}{R_{\text{ref}}} = \frac{R_{\text{ant}} - R_{\text{ref}}}{R_{\text{ref}}}, \qquad (1)$$

where R_{ant} is the spectrum reflected by the patch antenna and R_{ref} that of a reference consisting of a gold surface and the dielectric layer without Au disk (Fig. 4a). Because the only difference between antenna and reference is the presence of the Au disk, DRS quantifies the decrease of reflectivity, and therefore the relative absorption due to the presence of Au nanodisk with respect to the Au substrate and dielectric layer.

We performed multiple measurements for different patch nanoantennas exhibiting different shapes and diameter but equal dielectric layer thickness value of 40 nm. In Fig. 4b we show the differential reflectivity spectra of seven patches. We observe that all curves are characterized by a predominant dip around 500 nm.

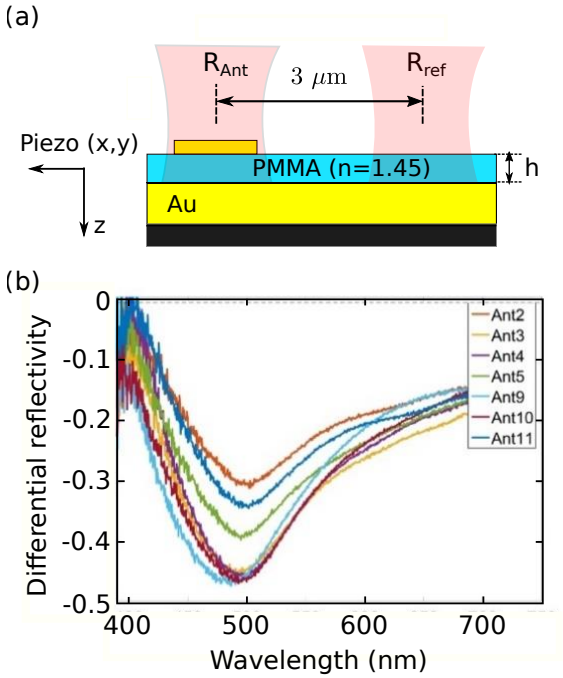

FIG. 4. Differential reflectivity spectra of single patch antennas. (a) Scheme of illumination for the measurements of the reflectivity of the patch antenna and reference areas. (b) Differential reflectivity spectra of the different patch antennas within the array, measured individually. The thickness of PMMA is h = 40 nm and the effective diameter of the antennas is reported in Fig. 5.

At this wavelength, the DRS varies between 30% and 50%, reaching almost an efficiency of 50% for antennas 4, 9, and 10. The error bars on the graphs in Fig. 5 represent the standard deviation of five consecutive measurements on the same antenna in order to get rid of lamp intensity fluctuations. Some antennas exhibit similar effective diameter but substantial difference in DRS. This feature is the case of Ant 2 and 10, with 30% and 47% of extrema values of DRS, respectively. Beyond the main absorption peak around 500 nm, the spectra present inflections and different slopes.

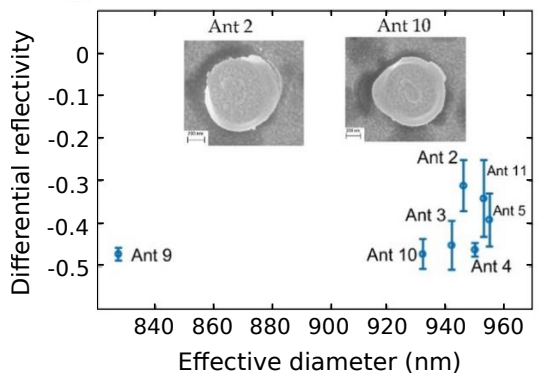

FIG. 5. Extrema DRS values. The error bars represent the standard deviation of five consecutive measurements.

To further investigate these antennas, we compare SEM and optical dark field images (Fig. 6). We see scattered light from the circular edge of the disks. In the case of the antenna 2, we distinguish a homogeneous blue ring around the nanostructure, whereas for antenna 10 we clearly observe a bright white spot on the left-side. This scattering spot is directly related with the asymmetry defect observed in the SEM image.

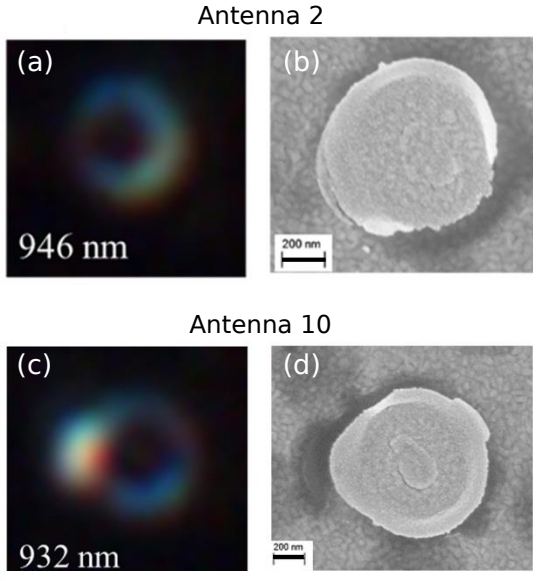

FIG. 6. Influence of asymmetrical path antennas on reflectivity measurements. (a) Optical dark-field and (b) scanning electron microscope images of antenna 2 with effective diameter 946 nm. (c) Optical dark-field and (b) SEM images of antenna 10 with effective diameter 932 nm. Patch antennas with equivalent effective diameter exhibit different DRS.

These results imply the influence of features such as asymmetric defects on the edges that induce hot spot increasing absorption displayed on reflectivity analysis.

To model the DRS of the antenna, we first consider the patch antenna as infinite in transverse direction by replacing the thin Au disk by an infinite Au layer of same thickness. We calculate numerically the reflection of a non-polarized plane wave normally incident on this "infinite patch" and on the reference one (i.e. without the top Au layer). One-dimensional finite-difference time-domain method, implemented by Meep[21], was used to numerically calculate the reflectivity spectra. The dielectric layer index was 1.45, corresponding to PMMA.

Figure 7a shows the results of the numerical calculations of the reflectance in different configurations: bare Au substrate, "infinite patch" in the case of 40 nm and 60 nm dielectric layer thickness. The differential reflectivity spectroscopy for both systems is calculated according to Eq. (1) and plotted in Fig. 7b. Both graphs reproduce well the experimental results (Fig. 4b). We observe a dip around 500 nm with values in differential reflectivity of DRS = -0.3 and DRS = -0.8 for 40 nm and 60 nm dielec-

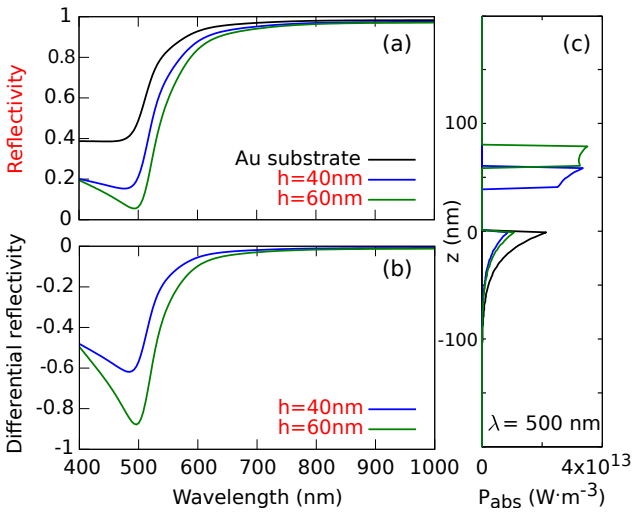

FIG. 7. "Infinite patch" antenna analysis. (a) Calculated reflectivity of a gold substrate, 40-nm-thick (solid green line) and 60-nm-thick (solid blue line) dielectric layer on gold substrate. (b) Calculated differential reflectivity spectra of "infinite patch" antennas with 40 nm and 60 nm dielectric layer obtained from (a). (c) Spatial distribution of the power dissipated by the gold "infinite patch" antennas and substrate.

tric thickness, respectively. By comparing both curves, we can observe that the increase of the thickness in the dielectric layer modifies the amplitude of the DRS dip but not the wavelength position. At this point, we will turn our discussion towards two main points: the origin of the dip at $\lambda = 500$ nm and the DRS variation with thickness dielectric layer. Figure 7a shows that the absorption of gold changes quickly within the interval 500 nm $< \lambda <$ 550 nm, but is quite flat for $\lambda <$ 500 nm, and for $\lambda >$ 550 nm. This is in accordance with the calculated DRS shown in Fig. 7b: the appearance of the dip around $\lambda = 500$ nm corresponds mainly to this abrupt change in the absorption properties of the gold material (see suppl. info.) whereas the DRS remains smooth for both regions exhibiting slight variation of the absorption. Indeed, the differential reflectivity spectroscopy estimates the relative difference between reference reflectivity and the curves "infinite patch" reflectivity in Fig. 7a. The differential reflectivity curves of Fig. 7b shows that the DRS of the antenna with 60 nm of dielectric layer is larger than that for 40 nm, as the resonance and spatial distribution of energy are not equivalent in both configurations. To evaluate the absorption dissipated by the "infinite patch" at $\lambda = 500$ nm, we calculated the power absorbed per unit volume across the antennas (Fig. 7c), defined as[22]:

$$P_{abs}(z,\omega) = -0.5\omega_0 |\mathbf{E}(z,\omega)|^2 \mathrm{Imag}[\epsilon(z,\omega)]\,, \qquad (2)$$

where ω_0 is the frequency, $\mathbf{E}$ is the electric field, and $\mathrm{Imag}(\epsilon)$ is the imaginary part of the Au permittivity. The total absorption in the volume is higher for the "infinite patch" with 60 nm gap than that with 40 nm.

This model is convenient to describe the main features in the reflectivity curve of those "infinite" patch nanoantenna. In this approach however, as it is based on the multiple interference between Au layers, any variation in size or shape of the nanostructures is not taken into account. To overcome this limitation for more realistic nanostructures simulations, we used 3D FDTD simulations. We used the full vectorial 3D FDTD method that supports the simulation of Maxwell's equations in cylindrical coordinates for the patch antenna that has continuous rotational symmetry around the z axis. The method is implemented by the freely-available software Meep[21]. By analogy with the Bloch's theorem, the field in a continuous rotational symmetry structure can be expressed as the field multiplied by an angular dependence in the form $\exp(\mathrm{i}m\phi)$ for some integer $m = 0, 1, 2, \ldots$, which is related to the angular momentum. Thus, the field can be expressed as:

$$\mathbf{E}(r,\phi,z) = \mathbf{E}(r,z)\exp(\mathrm{i}m\phi)\,. \qquad (3)$$

The field can be therefore expanded into its radial and azimuthal modes and identified with the indices (r, m), respectively. By placing a closed surface of flux monitors surrounding the nanoantenna, we calculate all incoming powers first without and then with the antenna. To obtain patch antenna absorption, we subtract the two results and normalize to the incident flux.

For the simulation, we use a linearly-polarized plane wave normally incident along the z direction. We first calculated the reflectance for the three different conditions presented beforehand: Au, 40-nm-thick dielectric layer on Au, and the reflectivity of a single nanoantenna of 1 μm in diameter (Fig. 8a). We can observe that the reflectivity response of the single antenna (40 nm thin dielectric layer) is quite similar to that of the reference calculated in the previous section (Fig. 7a). We observe that numerical results for the DRS dip around 500 nm agree roughly for finite size antenna ("infinite patch"). On the contrary, the DRS exhibit additional three dips around 600 nm, 709 nm, and 909 nm for the finite size patch, which are not present for the infinite patch. Because of the micrometer size of the structure, we attribute these dips to high-order resonance modes of the single patch. In the same Figure 8a we confirm that the maximum of absorption of the single nanoantenna corresponds to the peaks of the DRS for these 3 additional dips, whereas it is not the case for wavelengths around 500 nm, for which the absorption does not present a maximum but varies quickly with the wavelength. It confirms the fact that the dip in DRS at that wavelength is not due to the resonance of the finite size of the patch but is a signature of the abrupt change of gold absorption in the vicinity of $\lambda = 500$ nm. While the peaks at 709 nm and 909 nm are outside our detection bandwidth, the peak at $\lambda = 600$ nm is weakly detected (Fig. 4). To understand this feature and to investigate the influence of the radius size and edge defects on the DRS and absorption properties of the

patch antennas, we conducted FDTD simulations. The spectra red-shift for higher radius size, with 14.8 nm shift for every 10 nm increase on the radius. Gold edge defects also generate a red-shift but with higher values when the defect is placed at the upper-half height of the patch antenna relative to that placed at the middle. In contrast, dielectric defects do not produce any significant change (see suppl. info.). These simulations demonstrate that the consequences of various defects in real antennas is a broadening and flattening of absorption peaks, experimentally smoothing the weak peak around 600 nm.

To identify the modes of the field that we excite, we record the distribution of the mode fields at the resonant frequencies (Fig. 8). The mode fields are mainly oriented along the vertical z-axis with main component E_z.

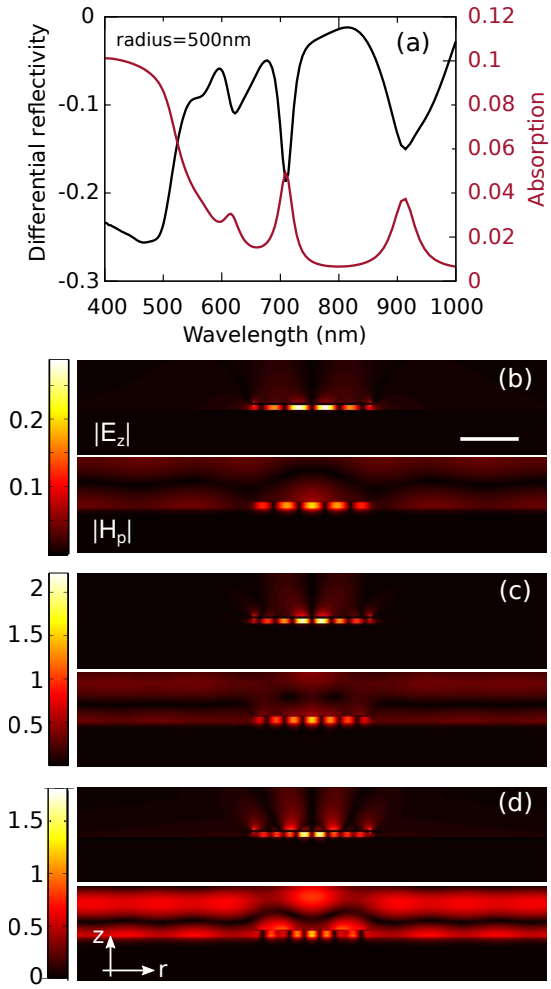

FIG. 8. Electromagnetic simulations of a gold patch antenna (radius = 500 nm). (a) Calculated differential reflectivity spectroscopy and absorption of the patch antenna. Distribution around the patch antenna of the z-component of the electric field and the ϕ-component of the magnetic field at wavelength (b) λ = 909.93 nm, (c) λ = 709.02 nm, and (d) λ = 615.64 nm. Scale bar is 500 nm in (b)-(d).

We confirm that high-order modes are excited as r = 2, 3, and 4 (Fig. 8b). However, the azimuthal index m is not clearly identified with the distribution of the modes. We suppose that the azimuthal index is m = 1 as the excitation a plane wave oriented along the r axis. In other words, dipoles are excited preferentially. In Figure 9, we plotted the angular dependencies of the mode field for r = 2, 3, 4 with m = 1.

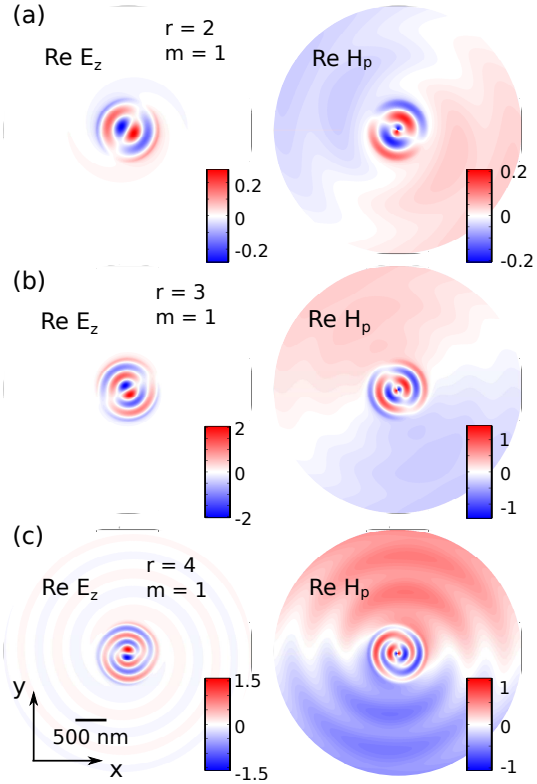

FIG. 9. Calculated real part of the z-component of the electric field and ϕ-component of the magnetic field at (a) 909.93 nm (r = 2), (b) 709. 02 nm (r = 3), and (c) 615.64 nm (r = 4). The azimuthal index is m = 1.

In summary, we described the experimental setup used to perform differential reflectivity spectroscopy on single nanoantennas. The DRS compares the absorption loss of the metallic nanoantenna with respect to a reference (i.e. a dielectric layer on a gold substrate) and quantifies the effect of the patch nanodisk. We found that for nanoantennas fabricated with similar parameters, the shape, effective diameter, and wavelength of maximum absorption can be slightly different between each structure with qualitative similar DRS but quantitative difference for the DRS maximum value. Indeed, they may present some non symmetric morphological defects inducing hot spots which have an influence on the absorption properties of the antenna and therefore on the DRS. Based on numerical simulations, we found that the amplitude of the differential reflectivity is strongly dependent of the dielectric gap between the metallic layers. Additionally, FDTD simulations of single patch antennas

reveal the excitation of additional resonance modes, observed only for finite-size antennas. This surface method provides an efficient tool to characterize the optical response of a nanostructure and offers this flexibility for other structured materials.

ACKNOWLEDGMENTS

Computations were carried out with the resources of the French Regional Grand-Est HPC Center ROMEO. J. U. E. would like to thank Loïc Becerra for technical assistance in SEM measurements.

DATA AVAILABILITY

The data that support the findings of this study are available from the corresponding author upon reasonable request.

REFERENCES

[1]R. Hummel and T. Dubroca, "Differential reflectance spectroscopy in analysis of surfaces," (American Cancer Society, 2014) pp. 1–25.

[2]R. Lazzari, J. Jupille, and Y. Borensztein, "In situ study of a thin metal film by optical means," Applied Surface Science **142**, 451–454 (1999).

[3]D. Martin, J. Jupille, and Y. Borensztein, "Silver particle sizes and shapes as determined during a deposit by in situ surface differential reflectance," Surface Science **402-404**, 433–436 (1998).

[4]L. Simonot, D. Babonneau, S. Camelio, D. Lantiat, P. Guérin, B. Lamongie, and V. Antad, "In situ optical spectroscopy during deposition of Ag:Si3N4 nanocomposite films by magnetron sputtering," Thin Solid Films **518**, 2637–2643 (2010).

[5]W. L. Mochán, R. G. Barrera, Y. Borensztein, and A. Tadjeddine, "Optical reflectance anisotropy of Ag and Au (110) single crystals," Physica A: Statistical Mechanics and its Applications **207**, 334–339 (1994).

[6]D. E. Aspnes and A. A. Studna, "Anisotropies in the above—band-gap optical spectra of cubic semiconductors," Phys. Rev. Lett. **54**, 1956–1959 (1985).

[7]C. Beitia, Y. Borensztein, R. G. Barrera, C. E. Román-Velázquez, and C. Noguez, "Multipolar plasma resonances in supported alkali-metal nanoparticles," Physica B: Condensed Matter **279**, 25–28 (2000).

[8]C. E. Román-Velázquez, C. Noguez, and R. G. Barrera, "Substrate effects on the optical properties of spheroidal nanoparticles," Phys. Rev. B **61**, 10427–10436 (2000).

[9]M. Kaniber, K. Schraml, A. Regler, J. Bartl, G. Glashagen, F. Flassig, J. Wierzbowski, and J. J. Finley, "Surface plasmon resonance spectroscopy of single bowtie nano-antennas using a differential reflectivity method," Scientific Reports **6**, 23203 (2016).

[10]H. T. Beyene, J. W. Weber, M. A. Verheijen, M. C. M. van de Sanden, and M. Creatore, "Real time in situ spectroscopic ellipsometry of the growth and plasmonic properties of Au nanoparticles on SiO_2," Nano Research **5**, 513–520 (2012).

[11]J. Proust, N. Bonod, J. Grand, and B. Gallas, "Optical monitoring of the magnetoelectric coupling in individual plasmonic scatterers," ACS Photonics **3**, 1581–1588 (2016).

[12]G.-C. Li, Q. Zhang, S. A. Maier, and D. Lei, "Plasmonic particle-on-film nanocavities: a versatile platform for plasmon-enhanced spectroscopy and photochemistry," Nanophotonics **7**, 1865 – 1889 (2018).

[13]T. Devkota, M. Devadas, A. Brown, J. Talghader, and G. Hartland, "Spatial modulation spectroscopy imaging of nano-objects of different sizes and shapes," Applied Optics **55**, 796–801 (2016).

[14]M. S. Devadas, Z. Li, T. A. Major, S. S. Lo, N. Havard, K. Yu, P. Johns, and G. V. Hartland, "Detection of single gold nanoparticles using spatial modulation spectroscopy implemented with a galvo-scanning mirror system," Appl. Opt. **52**, 7806–7811 (2013).

[15]C. Noguez, "Surface plasmons on metal nanoparticles: The influence of shape and physical environment," J. Phys. Chem. C **111**, 3806–3819 (2007).

[16]K. L. Kelly, E. Coronado, L. L. Zhao, and G. C. Schatz, "The optical properties of metal nanoparticles: The influence of size, shape, and dielectric environment," J. Phys. Chem. B **107**, 668–677 (2003).

[17]I. O. Sosa, C. Noguez, and R. G. Barrera, "Optical properties of metal nanoparticles with arbitrary shapes," J. Phys. Chem. B **107**, 6269–6275 (2003).

[18]C. Belacel, B. Habert, F. Bigourdan, F. Marquier, J. P. Hugonin, S. Michaelis de Vasconcellos, X. Lafosse, L. Coolen, C. Schwob, C. Javaux, B. Dubertret, J. J. Greffet, P. Senellart, and A. Maitre, "Controlling spontaneous emission with plasmonic optical patch antennas," Nano Letters **13**, 1516–1521 (2013).

[19]A. R. Dhawan, C. Belacel, J. U. Esparza-Villa, M. Nasilowski, Z. Wang, C. Schwob, J.-P. Hugonin, L. Coolen, B. Dubertret, P. Senellart, and A. Maître, "Extreme multiexciton emission from deterministically assembled single-emitter subwavelength plasmonic patch antennas," Light: Science & Applications **9**, 33 (2020).

[20]Y. Molard, F. Dorson, K. A. Brylev, M. A. Shestopalov, Y. Le Gal, S. Cordier, Y. V. Mironov, N. Kitamura, and C. Perrin, "Red-nir luminescent hybrid poly(methyl methacrylate) containing covalently linked octahedral rhenium metallic clusters," Chemistry –A European Journal **16**, 5613–5619 (2010).

[21]A. F. Oskooi, D. Roundy, M. Ibanescu, P. Bermel, J. D. Joannopoulos, and S. G. Johnson, "Meep: A flexible free-software package for electromagnetic simulations by the FDTD method," Computer Physics Communications **181**, 687–702 (2010).

[22]J. D. Jackson, "Classical electrodynamics," (John Wiley & Sons, Inc., 1999) Chap. 6, pp. 262–264, 3rd ed.

SUPPORTING INFORMATION for

Differential reflectivity spectroscopy on single patch nanoantennas

Juan Uriel Esparza,[1] Amit Raj Dhawan,[1] Rafael Salas-Montiel,[2] Willy Daney de Marcillac,[1] Jean-Marc Frigerio,[1] Bruno Gallas,[1] and Agnès Maître[1, a)]

[1)] *Sorbonne Université, CNRS, Institut des Nanosciences de Paris, UMR 7588, 75005 Paris, France*

[2)] *Department of Physics, Mechanics, Materials and Nanotechnology, L2n CNRS ERL 7004, Université de Technologie de Troyes, 12 rue Marie Curie, 10004, Troyes, France*

(Dated: 11 November 2020)

This document provides supporting information concerning the influence of radius size and edge defects on the DRS and absorption spectra. In addition, we provide the gold permittivity used for calculations.

[a)] Electronic mail: agnes.maitre@insp.upmc.fr

GOLD PERMITTIVITY

The permittivity of gold was measured with the use of spectroscopic ellipsometry in a wavelength range ranging from 400 nm to 1000 nm. The measured data were fitted to the Lorentz susceptibility model, with five oscillators. The fitted values were used for FDTD calculations. Below is plotted the permittivity of the gold used in the experiments and simulations.

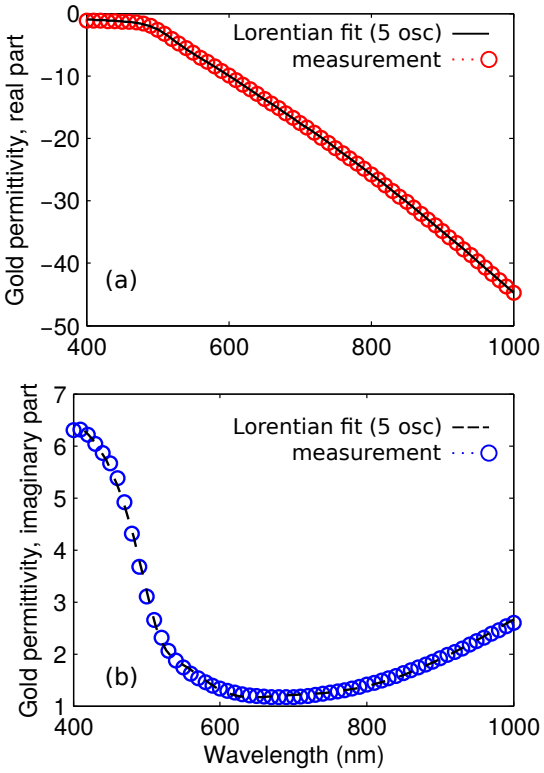

FIG. 1. Permittivity of gold in patch antennas. (a) Real and (b) imaginary parts of the permittivity of gold measured with spectroscopic measurement and fitted with five Lorentz oscillators used in FDTD simulations.

INFLUENCE OF RADIUS SIZE AND EDGE DEFECT OF THE PATCH ANTENNA ON THE DRS AND ABSORPTION SPECTRA

To investigate the influence of the radius size and edge defects on the DRS and absorption spectra of the patch antenna, we conducted FDTD simulations. The spectrum is red-shifted for higher radius size and edge defects.

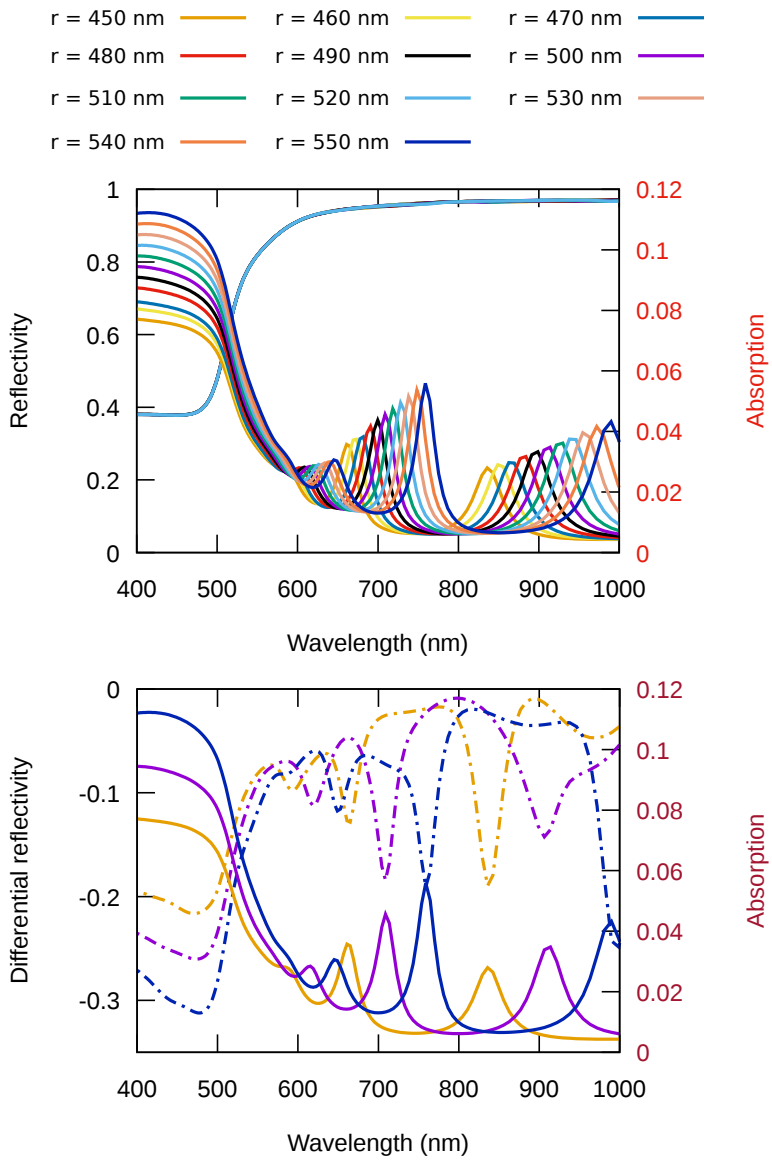

FIG. 2. Influence of the radius size on the DRS and absorption spectral properties of patch antennas.

We also performed numerical calculations of the influence of PMMA edge defects on the DRS and absorption spectra (Fig. 5).

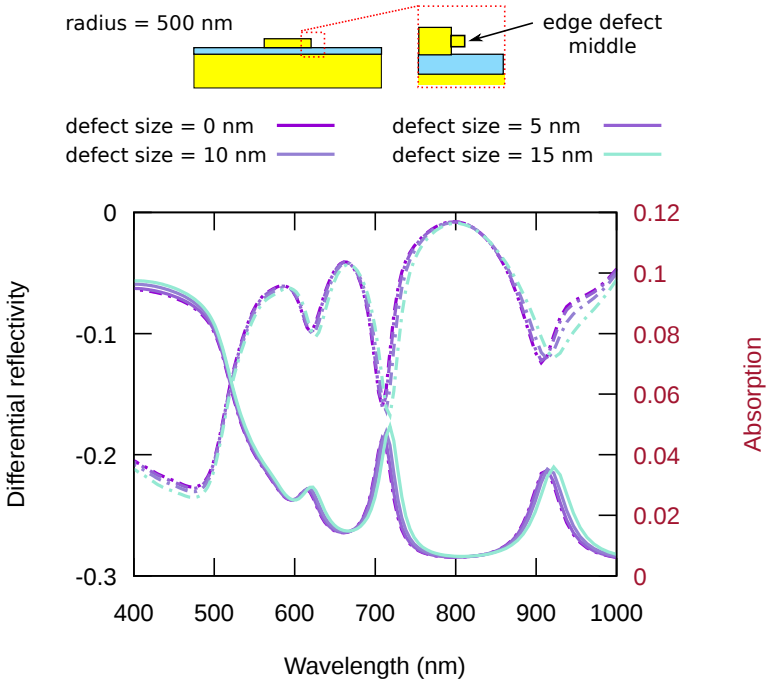

FIG. 3. Influence of edge defects on the DRS and absorption of patch antennas. An antenna with radius 500 nm and with squared edge defect at the middle height.

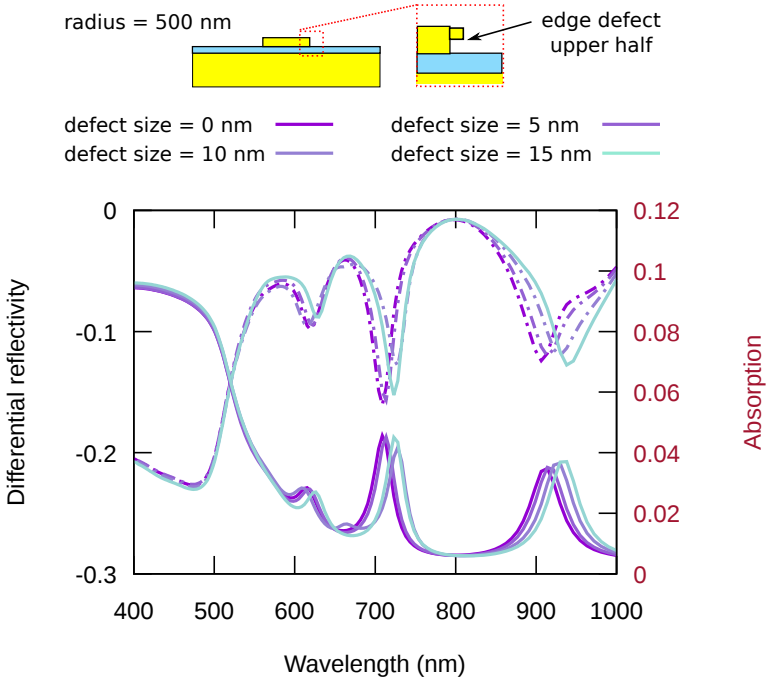

FIG. 4. Influence of edge defects on the DRS and absorption of patch antennas. The edge defect is placed at the upper half height of the patch antenna. The simulations were conducted with patch antenna with radius 500 nm.

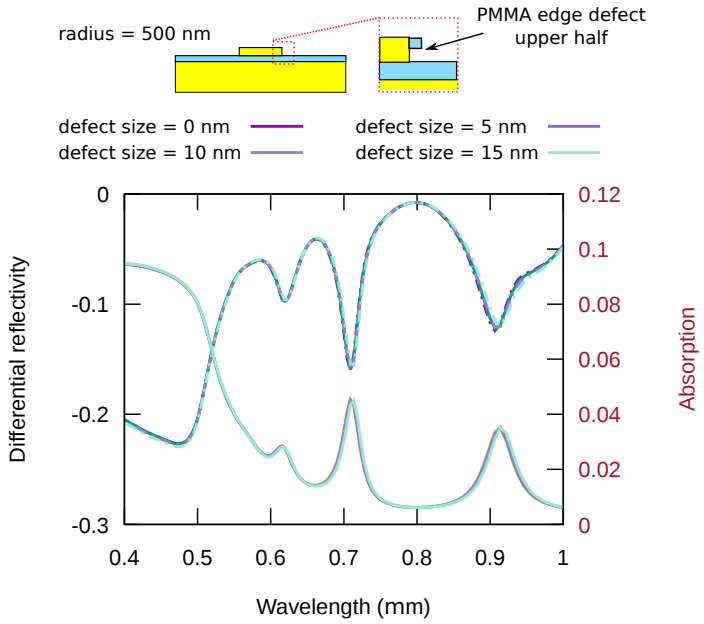

FIG. 5. Influence of PMMA edge defects on the DRS and absorption of patch antennas. The edge defect is placed at the upper half height of the patch antenna. The simulations were conducted with patch antenna with radius 500 nm.

No significant changes were obtained for PMMA edge defects on the DRS.